Advanced Laboratory Course

K221 – Mößbauer Effect

DOMINIC SCHÜCHTER[*] and JAKOB KRAUSE[†]

[*]✉ dschuechter@uni-bonn.de | ⭘ dschuechter

[†]✉ krause.jakob@uni-bonn.de | ⭘ krausejm

May 19. 2021

Abstract

In this report we investigated the MÖSSBAUER effect – a recoilless emission/absorption of photons by nuclei. We used the ^{57}Co isotope that decays into the excited ^{57}Fe and investigated it's 14.4keV line as a result of the transition between the first excited to ground state. Further we used the taken MÖSSBAUER spectrum to derive properties of electric and magnetic single and multipole properties like the g-factor and the natural linewidth Γ.

Contents

1 Introduction

In this experiment we investigated the recoilless γ emission and absorption of nuclei, the so called MÖSSBAUER-effect. With the used techniques of this experiment we were able to measure the natural linewidth of the ^{57}Fe transition to ground state at 14.4keV and investigate electric and magnetic single and multipole influences. Additionally we derived the LANDE-factor g for the hyperfine structure of the ground and first excited state of this isotope.

This lab report will introduce you into the fundamental theories behind the MÖSSBAUER-effect and -spectroscopy. The used experimental setup will be explained and the taken data presented and analyzed. Finally we briefly summarize the results and compare them to the literature values.

2 Theory

In this section we will give a brief introduction into the theory behind this experiment. This only gives the most important informations and equations needed for the later analysis. Knowledge of the DOPPLER-effect is required. For more detailed informations look e.g. [1] or [8].

2.1 Mößbauer effect

The MÖSSBAUER-effect is –as introduced– the recoilless emission/absorption of photons by nuclei. The fundamentals of physics are based on energy and momentum conservation. If a free, resting and excited nucleus transitions into its ground state via emitting a photon, its momentum changes in the opposite direction to the emitted photon. The energy of the photon is therefore smaller then the energy difference between the excited and ground state. If this photon encounters another free, resting nucleus at ground state of the same kind, the energy would now be to small to excite it. The same goes for a photon with a matching energy and a free, resting nucleus in ground state. Again –because of momentum conservation– would the energy of the photon converted into kinetic energy of the nucleus. For free, resting nuclei would therefore a resonant transition not be possible.

The MÖSSBAUER-effect gives a smart workaround for this problem. If the nuclei are part of a crystalline structure, the recoil energies are transferred into the whole crystal. The recoil becomes negligible for the high crystal mass. Resonant transitions are possible. [1]

2.2 Debye-Waller-factor

The DEBYE-WALLER-factor f is defined as the ratio between the recoilless emitted/absorbed γ's to all and is therefore the probability of the MÖSBAUER-effect [1]. For low temperatures ($T < \Theta$) the DEBYE-WALLER-factor can be written as [8]:

$$f(T) = \exp\left\{-\frac{\hbar^2 \cdot k^2}{2M}\frac{3}{2k_B\Theta}\left[1 + \frac{2\pi^2}{3}\left(\frac{T}{\Theta}\right)^2\right]\right\}$$

with the DEBYE-temperature Θ, temperature T, the atom mass M, BOLTZMANN. constant k_B

In general is this factor anti proportional to the temperature T and the photon energy E_γ ($\hbar \cdot k = \frac{E_\gamma}{c}$). The DEBYE-WALLER-factor is an important property of the used material. [8]

With the DEBYE-temperature for Iron $\Theta_{\text{Fe}} = 470K$ [5] and the energy $E_\gamma = 14.4keV$ follows:

$$f(T) \approx 0.78$$

This value is a good sign for the material choice, since we get at room temperatures sufficient values. One could improve this result by cooling done the source and absorber.
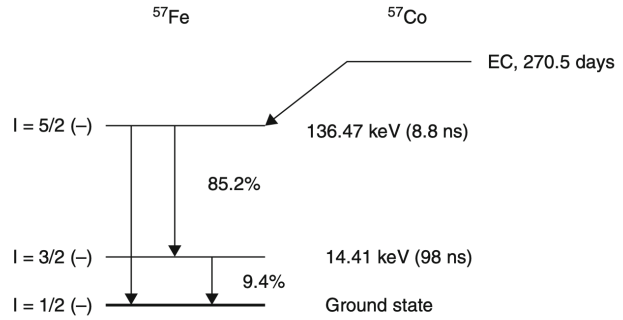
2.3 The Mößbauer-source – ^{57}Co-Decay scheme

A proper source to measure the MÖSSBAUER-spectrum requires the following properties [8]:

1. The observed γ-transition must lead to the ground state.

2. The Debye-Waller-factor should not be small

3. Practical lifetimes of the MÖSSBAUER-level because of resulting high linewidths $\Gamma = \frac{\hbar}{\tau}$

4. Practical properties of the parent isotope like the lifetime (continuous measurement)

Figure 1: ^{57}Co $\rightarrow$ ^{57}Fe decay scheme [1]

All those properties are fulfilled for the parent isotope ^{57}Co and the decay product (electron capture) ^{57}Fe. The decay scheme is show in figure 1. The resulting *coarse* γ-spectrum will contain three peaks. The resulting electron cascade will lead to a photopeak at $\approx$ 6keV, the peak of interest at 14.4keV and the simultanious measurement of both events. The transition from $|I = 5/2\rangle \rightarrow |I = 3/2\rangle$ or $|I = 5/2\rangle \rightarrow |I = 1/2\rangle$ result in energies that are not of interest and experimental configuration.

The transition of interest is the MÖSSBAUER-level $|I = 3/2\rangle$ to ground state $|I = 1/2\rangle$ which results in a photon with energy of 14.4keV. The transition time is long enough to build a sharp line profile. [8]

2.4 The Mößbauer-spectrum and its influences

The MÖSSBAUER spectrum isn't just a single line at 14.4keV. There are multiple effects due to electric and magnetic mono- and multipole effects happening [1]:

- **magnetic dipole interaction** Because our probe nuclei are embedded in iron, the ferromagnetic properties of iron apply. The internal magnetic field results in a hyperfine splitting. This results in two hyperfine levels for the ground state with the properties $|I = 1/2, m_I = \mp 1/2\rangle$ and in four levels for the MÖSSBAUER-state $|I = 3/2, m_I = \{\pm 1/2, \pm 3/2\}\rangle$. With the selection rule $\Delta m_I = 0, \pm 1$ [3] results a hyperfine spectrum of 6 discrete lines. The splitting of the energy can be calculated by the equation

$$\Delta E_I = -g_I \cdot B \cdot \mu_N \cdot \Delta m_I \tag{1}$$

  Figure 2 depicts the hyperfine scheme and the expected spectrum.

- **electric monopole interaction** Because of the nucleus size difference between the excited and ground state, an energy shift occurs due to coulomb interaction primary with lower level electrons. This shift is also called isomeric shift and leads to an asymmetry of the the MÖSSBAUER-spectrum as shown in figure 2 and described by [1]

$$\Delta E_{\text{iso.}} = E_\gamma^{A*} - E_\gamma^A \tag{2}$$

  The shift can therefore be easily (as we will later see) derived. [1]

- **electric quadrupole interaction** Because of nonzero nuclear quadrupole moments, our used isotopes are subject to electric quadrupole interaction which are characterized by the electric field gradient. This interaction also results in an energy shift of our spectrum. The resulting

shift can be described by the equation

$$\Delta E_Q \propto 3m_I^2 - I(I+1) \tag{3}$$

For the ground state with $I = 1/2$ and $m_I = \mp 1/2$ results a quadrupole shift of $\Delta E_Q = 0$. [1]
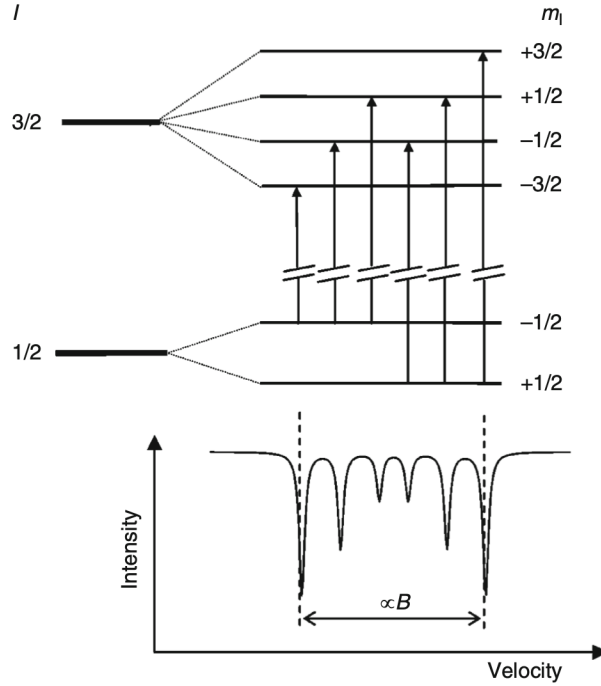
Figure 2: Magnetic dipole interaction/Hyperfine structure of the ground and first excited state of ^{57}Fe
[1]

Since our spectrum is the result of resonant absorption/transition the linewidth doesn't get affected by the DOPPLER broadening and the natural linewidth remains. The natural linewidth is of order 10^{-8}eV, while a broadened line is about 10^{-2}eV. Such small linewidth are really hard or impossible to capture with normal detectors without additional work. We will use a smart and surprisingly small setup to do so. [1]

3 Experimental Setup

The main idea to measure such small linewidths with high accuracy is to use the DOPPLER effect. An absorber and a source have resonant transitions. One can scan the peak profile by moving either the source or the absorber to or from the other. By doing so, the wavelength shifts and therefore the frequency of the emitted/received photon. The overlap of the absorber and emitter profiles are directly settling down in the counting rate. Since we measure after the absorber and take an absorption spectrum, the result shall be, that a higher overlap results in a lower counting rate. Figure 3 illustrates this idea. Since the movement is bidirectional and the spectrum is (besides single/multipole influences) symmetric, we can scan through the whole velocity spectrum. [1]

We used in our case a moving absorber with a ^{57}Fe target and a ^{57}Co source that is embedded in a metallic matrix. The source was covered by a box with an opening in direction of the absorber and detector. A gasdetector was used to measure the counting rate of γ's that is proportional to the voltage amplitude. The motor is controlled by a motorsteering which had a potentiometer to control it's velocity and got gate signals from further electronics (Part 2). Because of the bidirectional configuration, one needs two separate counters. The first one for the movements direction from left to right (LR) and the second one for the movement from right to left (RL). The setup could not guaranty the same speed in LR and RL directions, even with the same steering settings. Therefore was for every run also the time besides the number of counts measured, from which the counting rate and velocity could be calculated. This time information came from an variable timer. With a run counter could the number of rounds be counted. A full round starts at the maximal left position and can't be interrupted by the electronics. Only the number of rounds can be controlled. With an SCA can be an energy spectrum taken or an energy window set (Part 1). Figure 4 shows a principle schematic of the setup. [6]
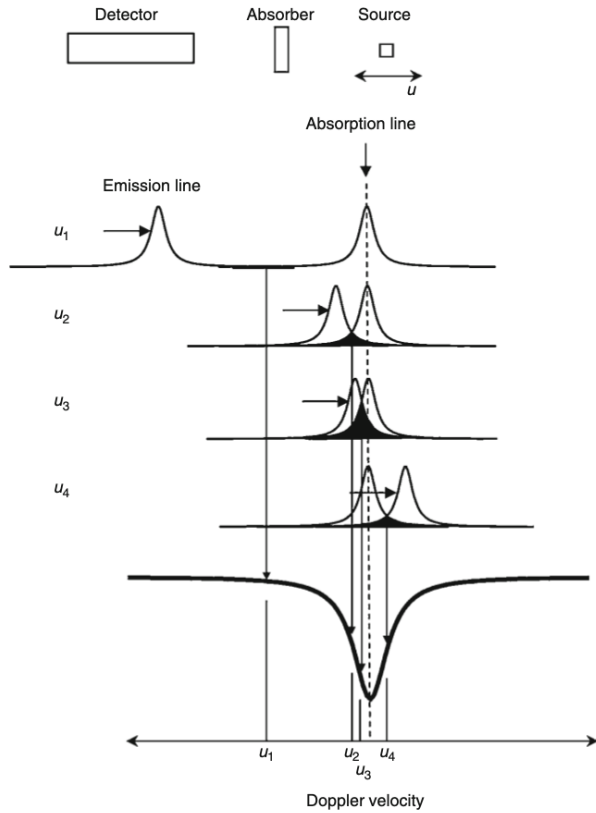
Figure 3: Main idea of MÖSSBAUER-spectroscopy [1]
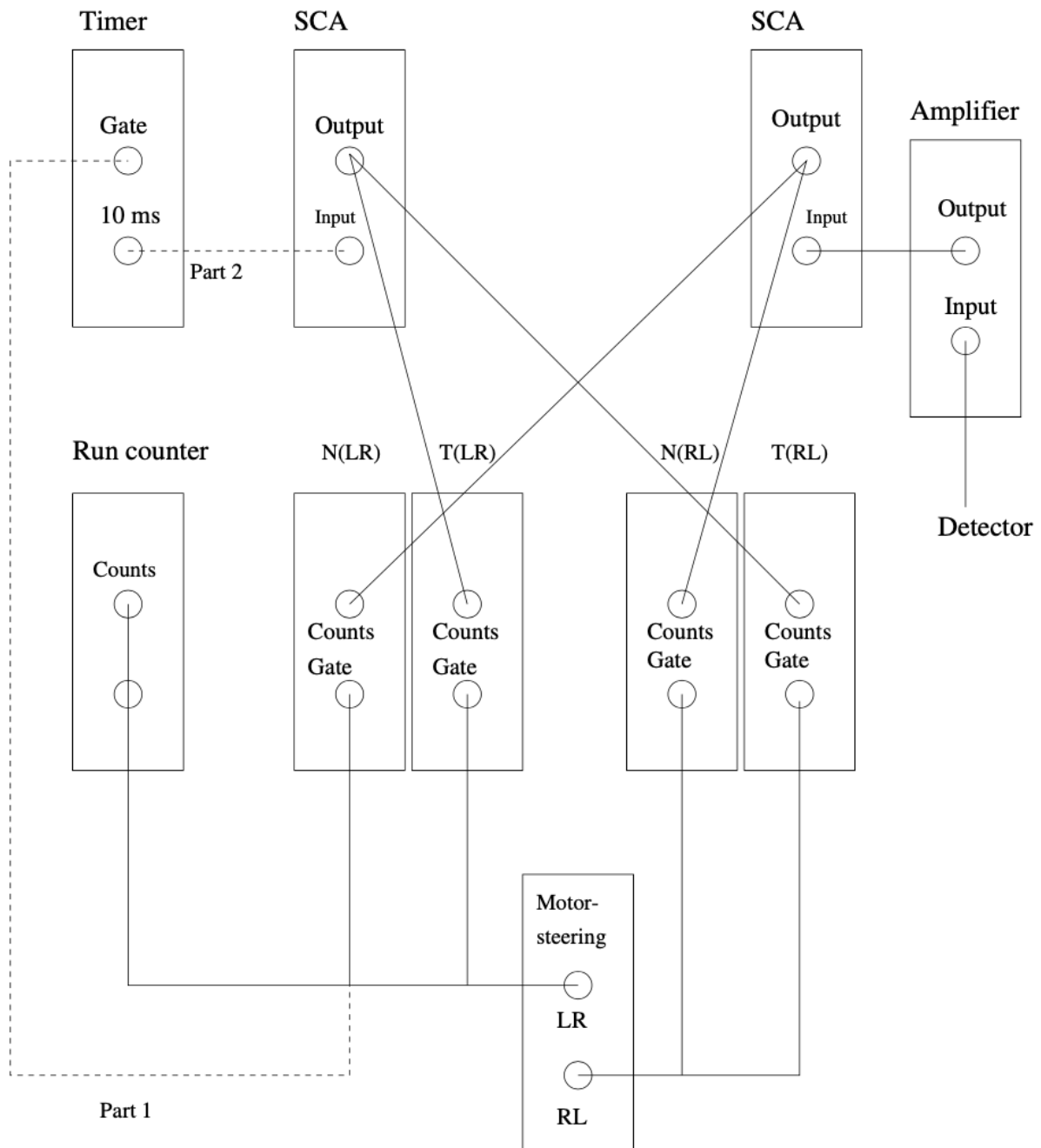
Figure 4: Experimental setup with the two wiring option Part 1 and Part 2 [6]

4 Measurements and Analysis

In this section we will present our measurement and do the analysis of the data.

4.1 Measurement of the ^{57}Fe γ-spectrum

After the initial setup, we wired the electronics to match Part 1 from scheme 4. With this setup we are able to measure the γ-spectrum of ^{57}Fe and set a proper window size of the SCA. To get a sufficient resoluted spectrum, we set the window size to 50 Channel-Units and increased –after every 10s measurement of the counting rate– the lower limit. Because we couldn't set the potentiometer to 0 Ch. on the SCA, we started at 100 Ch.. We scanned for three lines. The first would be the energy of the electron cascade that happens after the electron capture in the ^{57}Co at about 6keV, the second should be the MÖSBAUER-line –that we are searching for– of 14.4keV and a third small one, that is a result of the simultaneous measuring (detector limitation/coincidences) of the first two lines at the sum of both energies. The resulting histogram is shown in figure 5.
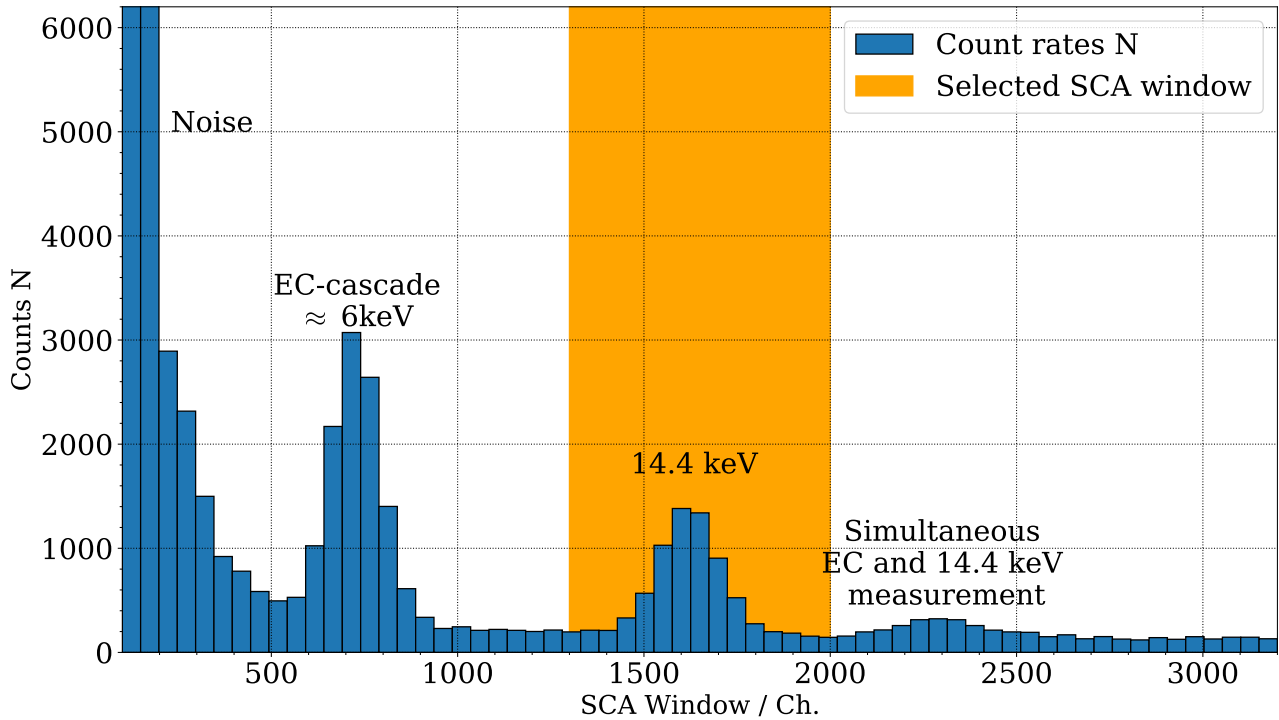
Figure 5: γ-spectrum of ^{57}Fe

For the following measurement we set the SCA window to 1300-2000 Ch..

4.2 Measurement of the MÖSSBAUER-spectrum

After setting the SCA-window, we proceeded by wiring up Part 2 of scheme 4. Therefore we applied the gate signal of the timer to the counter NL.

The motorspeed can be set by a potentiometer. We started with the highest possible velocity (2.60 Ch.). One could also start with the slowest but since we didn't know in which velocity space the

absorption dips are visible and the velocity is given in units of mm/s, the waiting times for one round would be extremely long. For the coarse measurement of the background we chose 0.04 Ch. steps and for measurements inside the dip 0.02 Ch.. Our goal was to measure for each velocity at least 4000 events s.t. the resulting relative error of the counting rate is < 2%. The resulting MÖSBAUER-spectrum is depicted in figure 6.
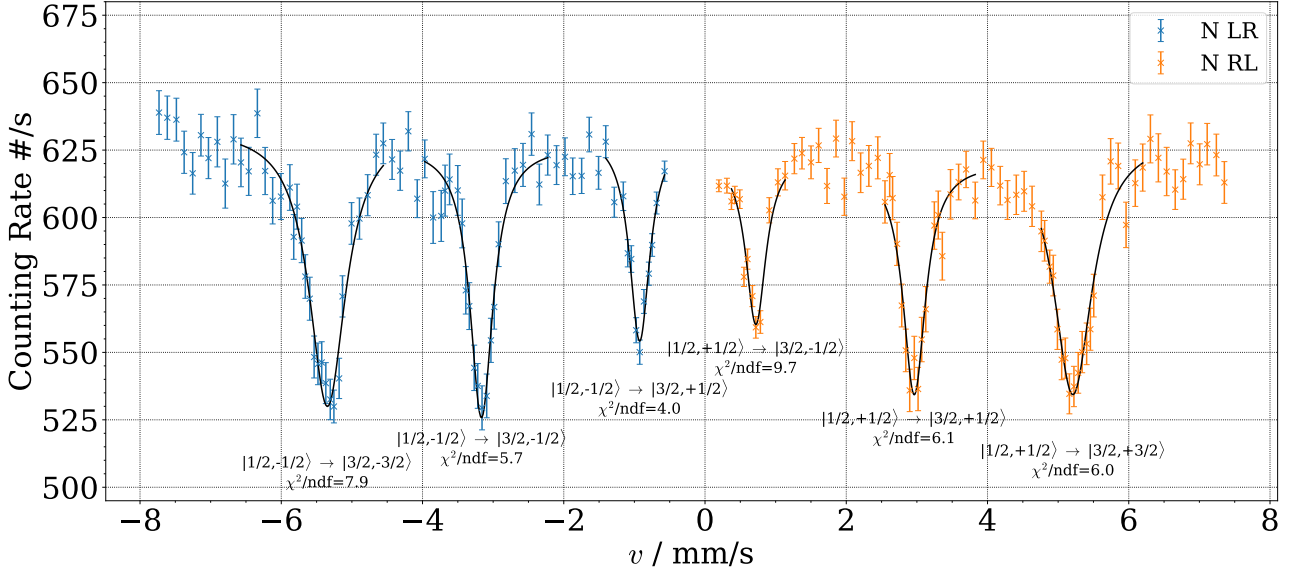
Figure 6: MÖSSBAUER-spectrum of the 14.4keV line of ^{57}Fe. The dip labels refer to $|I, m_I\rangle$

We applied the convention that positive velocities mean approaching source and absorber or in other words, the movements from right to left (RL) [1]. The velocity was calculated from the known distance $s = 25.1$mm, the time t and the number of rounds N_r. The electronics are set up in away, that a round starts on the left side and makes at least one full round trip.

One can see that we didn't measure even smaller velocities because of time reasons and the knowledge that there should only be 6 dips for this spectrum. We then fitted the LORENTZ-function [2]

$$f(v) = a \cdot \frac{(\frac{\Gamma}{2})^2}{(v - v_0)^2 + (\frac{\Gamma}{2})^2} + b$$

with the linewidth Γ, the amplitude a, offset b and mean velocity v_0

to every dip and ordered them to the associated transitions. The observed linewidth Γ is twice as wide as the natural line width [1] why?. This can be done by assigning the expected relative dip heights –given by the the square of the corresponding $3j$ symbol [1]– to the measured ones. The derivation of the relation between the relative peak intensity I and the $3j$-symbol

$$I(I_e, m_e, I_g, m_g, \sigma lm) \propto \begin{pmatrix} I_g & l & I_e \\ -m_g & m & m_e \end{pmatrix}^2 F_{lm}(\theta)$$

would break the boundaries of this report. One can consult for further information the text book [1]. Table 1 lists all found parameters for every dip and the corresponding $3j$ symbol taken from [1].

Differences in velocity can be transferred in units of energy by [1]:

$$dE = \frac{dE}{dv}dv = \frac{E}{c}dv \Rightarrow \Delta E = \frac{14.4keV}{c}\Delta v$$

Transition $|I, m_I\rangle$	$3j$-square	a	b	Γ / mm/s	v_0 / mm/s
$|1/2, -1/2\rangle \rightarrow |3/2, -3/2\rangle$	3/12	-103.3 ± 5.4	633.3 ± 5.1	0.626 ± 0.071	-5.346 ± 0.013
$|1/2, -1/2\rangle \rightarrow |3/2, -1/2\rangle$	2/12	-100.8 ± 5.6	626.5 ± 3.7	0.394 ± 0.045	-3.165 ± 0.010
$|1/2, -1/2\rangle \rightarrow |3/2, +1/2\rangle$	1/12	-76.8 ± 6.6	630.9 ± 6.8	0.350 ± 0.055	-0.925 ± 0.009
$|1/2, +1/2\rangle \rightarrow |3/2, +3/2\rangle$	3/12	-95.5 ± 7.3	629.9 ± 7.5	0.662 ± 0.090	5.209 ± 0.014
$|1/2, +1/2\rangle \rightarrow |3/2, +1/2\rangle$	2/12	-85.8 ± 6.7	620.0 ± 5.3	0.387 ± 0.065	2.963 ± 0.014
$|1/2, +1/2\rangle \rightarrow |3/2, -1/2\rangle$	1/12	-63.1 ± 10.3	623.4 ± 10.9	0.348 ± 0.116	0.720 ± 0.020

Table 1: Fit parameters for the associated dips

4.3 Line widths

After the conversion into units of energy the parameters of interest from table 1 become

Transition $|I, m_I\rangle$	Γ / neV	E_0 / neV
$|1/2,-1/2\rangle \rightarrow |3/2,-3/2\rangle$	30.068 ± 3.414	-256.623 ± 0.633
$|1/2,-1/2\rangle \rightarrow |3/2,-1/2\rangle$	18.907 ± 2.147	-151.934 ± 0.481
$|1/2,-1/2\rangle \rightarrow |3/2,+1/2\rangle$	16.814 ± 2.630	-44.405 ± 0.427
$|1/2,+1/2\rangle \rightarrow |3/2,+3/2\rangle$	31.793 ± 4.331	250.018 ± 0.677
$|1/2,+1/2\rangle \rightarrow |3/2,+1/2\rangle$	18.582 ± 3.140	142.210 ± 0.657
$|1/2,+1/2\rangle \rightarrow |3/2,-1/2\rangle$	16.720 ± 5.555	34.562 ± 0.937

Table 2: Fit parameters for the associated dips

and the spectrum looks as depicted in figure 7.
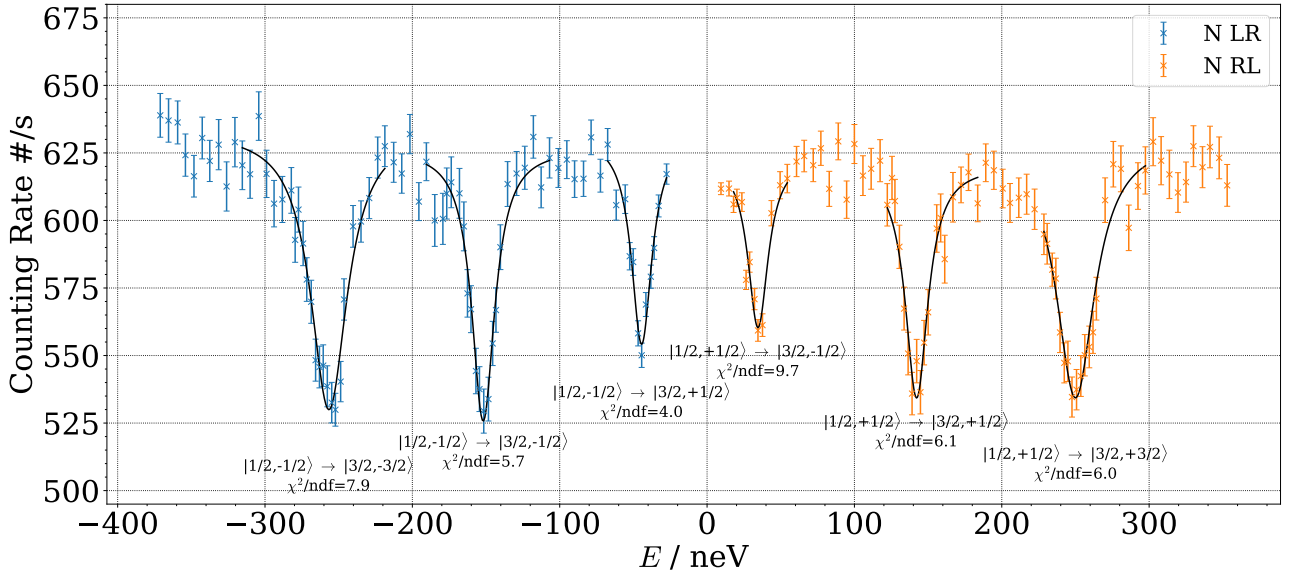
Figure 7: MÖSSBAUER-spectrum of the 14.4keV line of ^{57}Fe in units of energy. The dip labels refer to $|I, m_I\rangle$

The observed double linewidths lie between around 17 neV and 31 neV. As motivated in section 4.2 the linewidth of the absorption/emission only is the half measured width and lies between 8.5

neV and 15.5 neV. The known natural linewidth of the ^{57}Fe is 4.7neV [8] and therefore only 1.8-3.3 times smaller than our measurement. The broadening can be the result of a Debye-Waller-factor f that is <1. The tutor suggested that the factor is less then 80% –our estimation from section 2.2 was $f \approx 0.78$– which means that round 20% of all photons –emitted and absorbed– loose energy on phonons on either the source or the target material. The material choice, even with this Debye-Waller-factor is sufficient, since it doesn't require cooling and has long livetimes. A material with $f = 1$ can't be found even at temperatures of $T = 0$K due to zero-point energy. [8]

4.4 The g-factor

Now we want to derive the g-factors for the excited and ground state $g_{3/2}$ and $g_{1/2}$ from our data.

For the magnetic field of the ^{57}Fe we assume $H = (333 \pm 10)$kG $= (33.3 \pm 1.0)$T [6] and use the literature value for the nuclear magneton $\mu_N = 3.152451 \cdot 10^{-8}$eVT^{-1} [4] to derive with equation (1) the relations

$$g_{1/2} = -\frac{\Delta E_{1/2}}{\mu_N \cdot B} \qquad\qquad g_{3/2} = -\frac{\Delta E_{3/2}}{\mu_N \cdot B}$$

for splittings with $\Delta m_I = 1$ and the associated energy difference ΔE_I.

Our choice for the transitions depends –as explained in 2.4– on the fact, that we want to cancel out the quadrupole shift. Since for the ground state a quadrupole shift doesn't exist, we chose the transitions to the excited states $m_{3/2} = \pm 1/2$. The choice of states is intuitively depicted in figure 2. We find for each g-factor two energy differences ΔE_I:

$$\Delta E_{1/2} = \begin{cases} E(|1/2, +1/2\rangle \to |3/2, -1/2\rangle) - E(|1/2, -1/2\rangle \to |3/2, -1/2\rangle) \\ E(|1/2, +1/2\rangle \to |3/2, +1/2\rangle) - E(|1/2, -1/2\rangle \to |3/2, +1/2\rangle) \end{cases}$$

$$\Delta E_{3/2} = \begin{cases} E(|1/2, -1/2\rangle \to |3/2, +1/2\rangle) - E(|1/2, -1/2\rangle \to |3/2, -1/2\rangle) \\ E(|1/2, +1/2\rangle \to |3/2, +1/2\rangle) - E(|1/2, +1/2\rangle \to |3/2, -1/2\rangle) \end{cases}$$

By averaging those energies, one finds:

$$\Delta E_{1/2} = (-186.56 \pm 0.66)\text{neV} \Rightarrow g_{1/2} = 0.1777 \pm 0.0049$$
$$\Delta E_{3/2} = (107.59 \pm 0.66)\text{neV} \Rightarrow g_{3/2} = -0.1025 \pm 0.0038$$

To set the found values in comparison to the literature [7], we take the ratio between both found factors g_I:

$$G_{\text{exp.}} = \frac{g_{1/2}}{g_{3/2}} = -1.734 \pm 0.0625 \qquad\qquad G_{\text{lit.}} = -1.715 \pm 0.004$$

The literature value of $G_{lit.}$ lies within the error of our result. Besides this deviates our result by just $\approx 1\%$ from the literature value. This is a surprising accurate result.

4.5 Isomeric shift

By inverting the sign of the energies for LR, one can see that the spectrum isn't perfectly symmetric (see 8). This results from the isomeric shift that shifts the whole spectrum by ΔE_{iso}.

One can then derive the isomeric shift by calculating the shifts between each peak and his presumptive mirrored one. Since the signs of LR and RL are opposite this is the same as the average of all peak positions. With this in mind we find the isomeric shift

$$\Delta E_{\mathrm{iso.}} = (-4.36 \pm 0.80)\mathrm{neV}$$

The isomeric shift is probably the result of the different materials that the $^{57}\mathrm{Co}$ respectively $^{57}\mathrm{Fe}$ probes are held in.
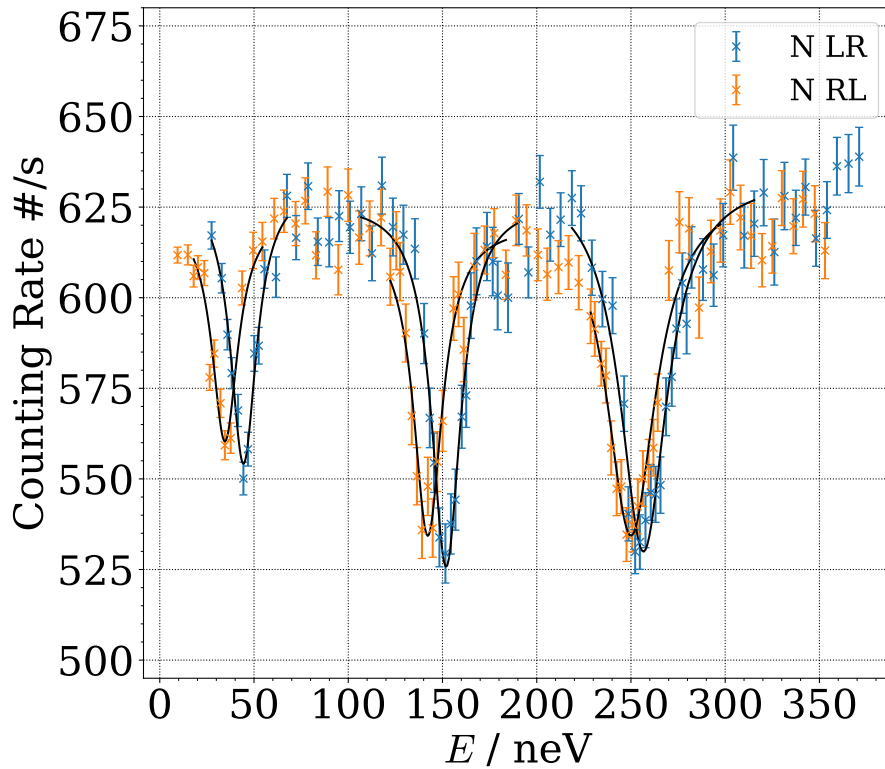
Figure 8: Mirrored LR measurement to visualize isomeric shift

5 Conclusion

In this lab course we investigated the recoilless absorption/emission called Mössbauer-effect. We started with taking a coarse γ-spectrum to find the 14.4keV transition of ^{57}Fe to calibrate the window of a single channel analyzer. Afterwards we measured with a source and a moving absorber the so called Mössbauer-spectrum that includes visible effects of electric and magnetic multipole effects.

One derived property of this spectrum is the natural linewidth, which was determined for the hyperfine structure and lied between 8.5neV and 15.5neV. Therefor was our result about 1.8-3.3 times larger then the known linewidth of 4.7neV [8].

From the resulting Mössbauer-spectrum we obtained the g-factor for the ground state and excited state as:

$$g_{1/2} = 0.1777 \pm 0.0049 \qquad\qquad g_{3/2} = -0.1025 \pm 0.0038$$

and compared the ratio of them to the literature value from [7]:

$$G_{\text{exp.}} = \frac{g_{1/2}}{g_{3/2}} = -1.734 \pm 0.0625 \qquad\qquad G_{\text{lit.}} = -1.715 \pm 0.004$$

Last but not least we investigated the isomeric shift that shifts the whole spectrum by the energy

$$\Delta E_{\text{iso.}} = (4.36 \pm 0.80)\text{neV}$$

The overall results are impressive, especially if one takes the small dimensions of the experiment and the slow velocities into account. We could have decreased the errors by measuring longer since the error of counts N goes with $\sqrt{N}$. The experiment was long not in use, therefore the electronics could have suffered from thermal influences. We countered this by letting it run for a few minutes before taking any measurements. The influence of thermal fluctuation was not significant.

6 Appendix

6.1 Remark on measurement errors

We measured counts throughout the whole experiment. Every count N is associated with an error $\sigma_N = \sqrt{N}$ (POISSON statistics). All errors are propagated using GAUSSIAN error propagation.

6.2 Measured data

All data we measured was visualized in this report only in the form of plots. If there is need to view the data in detail it can be found in our GitHub repository.

lower limit / Ch.	upper limit / Ch.	counts N	time t / s
100	50	71770	10
150	200	6954	10
200	250	2893	10
250	300	2317	10
300	350	1499	10
350	400	921	10
400	450	780	10
450	500	585	10
500	550	495	10
550	600	529	10
600	650	1024	10
650	700	2170	10
700	750	3072	10
750	800	2642	10
800	850	1402	10
850	900	612	10
900	950	337	10
950	1000	230	10
1000	1050	246	10
1050	1100	212	10
1100	1150	221	10
1150	1200	212	10
1200	1250	201	10
1250	1300	215	10
1300	1350	197	10
1350	1400	213	10
1400	1450	211	10
1450	1500	331	10
1500	1550	568	10
1550	1600	1029	10
1600	1650	1382	10
1650	1700	1340	10
1700	1750	905	10
1750	1800	525	10
1800	1850	275	10
1850	1900	199	10
1900	1950	185	10
1950	2000	156	10
2000	2050	145	10
2050	2100	157	10
2100	2150	197	10
2150	2200	216	10
2200	2250	258	10
2250	2300	314	10

Table 3: Data of Part 1

lower limit / Ch.	upper limit / Ch.	counts N	time t / s
2300	2350	323	10
2350	2400	314	10
2400	2450	258	10
2450	2500	214	10
2500	2550	197	10
2550	2600	193	10
2600	2650	151	10
2650	2700	169	10
2700	2750	131	10
2750	2800	152	10
2800	2850	128	10
2850	2900	120	10
2900	2950	142	10
2950	3000	126	10
3000	3050	151	10
3050	3100	129	10
3100	3150	146	10
3150	3200	146	10
3200	3250	131	10

Table 3: Data of Part 1

Velocity / Ch.	rounds	t_{LR} / 10ms	N_{LR}	t_{RL} / 10m	N_{RL}
2.6	3	974	6223	1024	6277
2.56	3	989	6300	1040	6481
2.52	3	1006	6401	1059	6642
2.48	3	1021	6373	1075	6662
2.44	3	1038	6398	1095	6871
2.4	3	1055	6652	1112	6830
2.36	3	1071	6662	1131	6903
2.32	2	727	4566	768	4739
2.28	2	739	4527	782	4865
2.24	2	752	4730	796	5008
2.2	2	764	4740	810	5010
2.16	2	777	4795	824	5049
2.12	2	792	5058	842	5029
2.08	2	806	4975	858	5312
2.04	2	820	4971	874	5426
2	2	836	5081	892	5419
1.96	2	854	5219	912	5208
1.94	2	862	5110	920	5139
1.92	2	869	5249	929	5139

Table 4: Data of Part 2

Velocity / Ch.	rounds	t_{LR} / 10ms	N_{LR}	t_{RL} / 10m	N_{RL}
1.90	2	879	5199	940	5171
1.88	2	887	5128	950	5153
1.86	2	897	5112	961	5164
1.84	2	907	4973	973	5202
1.82	2	916	4999	984	5391
1.8	2	925	5053	994	5440
1.78	2	935	5036	1006	5619
1.76	2	946	5038	1018	5889
1.74	3	1433	7594	1543	8977
1.72	2	969	5236	1044	6174
1.70	2	978	5582	1054	6270
1.66	2	1003	5996	1084	6549
1.62	2	1026	6152	1111	6774
1.58	2	1051	6393	1139	6930
1.54	2	1078	6719	1172	7108
1.50	2	1102	6915	1201	7348
1.46	2	1133	7042	1238	7658
1.42	2	1163	7180	1274	7916
1.38	2	1195	7552	1312	7955
1.34	2	1232	7478	1358	8390
1.30	2	1265	7865	1398	8572
1.26	1	652	3912	722	4394
1.22	1	672	4036	747	4375
1.2	1	682	4160	760	4567
1.18	1	694	4262	773	4615
1.14	1	717	4374	803	4545
1.12	1	730	4364	818	4538
1.1	1	741	4246	832	4463
1.08	1	752	4265	847	4641
1.06	1	768	4180	866	4641
1.04	1	780	4193	883	4863
1.02	1	795	4209	901	5112
1.0	1	812	4335	923	5448
0.98	1	828	4591	945	5738
0.96	1	841	4767	960	5911
0.94	1	859	5069	985	5967
0.9	1	890	5460	1026	6383
0.86	1	932	5754	1082	6699
0.82	1	974	6034	1139	7023
0.78	1	1022	6448	1205	7571
0.74	1	1070	6551	1272	7730
0.70	1	1127	7023	1353	8514
0.66	1	1194	7396	1453	8888
0.62	1	1266	7881	1560	9777
0.58	1	1340	8245	1672	10374

Table 4: Data of Part 2

Velocity / Ch.	rounds	t_{LR} / 10ms	N_{LR}	t_{RL} / 10m	N_{RL}
0.54	1	1437	8844	1828	11404
0.50	1	1531	9657	1984	12337
0.46	1	1665	10266	2213	13621
0.42	1	1786	11218	2431	14903
0.38	1	1954	11835	2757	16616
0.34	1	2169	13185	3203	17977
0.32	1	2295	13466	3488	19508
0.30	1	2404	14054	3742	21362
0.28	1	2575	14374	4172	24389
0.26	1	2715	14935	4551	26305
0.24	1	2902	16509	5102	30959
0.22	1	3156	18279	5950	36199
0.20	1	3354	19782	6704	40624
0.18	1	3665	22187	8092	49508
0.14	1	4385	27063	12765	78090

Table 4: Data of Part 2

References

[1]   Zoltan Klencsar Rezso G. Lovas Frank Rösch Attila Vertes Sandor Nagy. *Handbook of Nuclear Chemistry*. Springer Science+Business Media B.V., 2011.

[2]   W. Demtröder. *Laser Spectroscopy Vol. 1*. Springer, 2008.

[3]   Wolfgang Demtröder. *Experimentalphysik 4 – Kern-, Teilchen- und Astrophysik*. Springer Spektrum, 2017.

[4]   Particle Data Group. *Physical Constants (a major revision)*. URL: `https://pdg.lbl.gov/2020/reviews/rpp2020-rev-phys-constants.pdf`.

[5]   Charles Kittels. *Introduction to Solid State Physics*. John Whiley and Sons Inc., 2005.

[6]   o.V. *Script: K221 Mössbauer effect*. Nussallee 12, D-53115 Bonn: Universität Bonn, March 1998.

[7]   J. Heberle R. Preston S. Hanna. *Mossbauer Effect in Metallic Iron*. 1962. URL: `https://journals.aps.org/pr/pdf/10.1103/PhysRev.128.2207`.

[8]   Weidinger Schatz. *Condensed Matter Physics*. Teubner Verlag.